Advances in Nano Research, *Vol. 5 No. 4 (2017) 337-357*
DOI: https://doi.org/10.12989/anr.2017.5.4.337

An exact solution for mechanical behavior of BFRP Nano-thin films embedded in NEMS

Wael A. Altabey*[1,2]

[1] (*Current*) *International Institute for Urban Systems Engineering*, *Southeast University*, *Nanjing 210096*, *China*
[2] (*Previous*) *Department of Mechanical Engineering*, *Faculty of Engineering*, *Alexandria University*, *Alexandria* (*21544*), *Egypt*

(*Received November 30, 2016, Revised May 18, 2017, Accepted May 20, 2017*)

Abstract. Knowledge of thin films mechanical properties is strongly associated to the reliability and the performances of Nano Electro Mechanical Systems (NEMS). In the literature, there are several methods for micro materials characterization. Bulge test is an established nondestructive technique for studying the mechanical properties of thin films. This study improve the performances of NEMS by investigating the mechanical behavior of Nano rectangular thin film (NRTF) made of new material embedded in Nano Electro Mechanical Systems (NEMS) by developing the bulge test technique. The NRTF built from adhesively-bonded layers of basalt fiber reinforced polymer (BFRP) laminate composite materials in Nano size at room temperature and were used for plane-strain bulging. The NRTF is first pre-stressed to ensure that is no initial deflection before applied the loads on NRTF and then clamped between two plates. A differential pressure is applying to a deformation of the laminated composite NRTF. This makes the plane-strain bulge test idea for studying the mechanical behavior of laminated composite NRTF in both the elastic and plastic regimes. An exact solution of governing equations for symmetric cross-ply BFRP laminated composite NRTF was established with taking in-to account the effect of the residual strength from pre-stressed loading. The stress-strain relationship of the BFRP laminated composite NRTF was determined by hydraulic bulging test. The NRTF thickness gradation in different points of hemisphere formed in bulge test was analysed.

Keywords: bulge test technique; mechanical behavior; Micro/Nano Electro-Mechanical Sensors (MEMS/ NEMS); basalt fiber reinforced polymer (BFRP)

1. Introduction

The micro or Nano-size scale in diaphragm is the most important part in numerous engineering and bioengineering sensors applications such as the micro electro-mechanical sensors (MEMS) and Nano Electro Mechanical Systems (NEMS), e.g., the pressure sensors normally have a micro or Nano diaphragm that deforms in the presence of pressure difference.

Accurate measurement of materials properties in the fabrication of Micro Electro Mechanical Systems (MEMS) and more recently Nano Electro Mechanical Systems (NEMS) is a great challenge, especially when these properties depend on the fabrication process.

In addition, fast growing progress in the structural elements application such as diaphragm with

*Corresponding author, Professor, E-mail: wael.altabey@gmail.com

 ISSN: 2287-237X (Print), 2287-2388 (Online)

micro or Nano-size scale in MEMS/ NEMS, due to their outstanding chemical, mechanical, and electrical properties, led to a challenge in modelling of Micro/Nano scale structures. In such applications, it is presented that the size effect has a major influence on Mechanical behavior of material. The importance of size effects induced the scientific development for the behaviors of the Nano-structures and Nano-materials much accurately (Alizada and Sofiyev 2011a, b, 2012).

To understand the thermomechanical behavior of nanostructures, the numerous works for modeling and measurement of thermomechanical formation and thermal detection of nanostructures under vibration and buckling load (Ebrahimi *et al*. 2015, Ebrahimi and Salari 2015a, b, Ebrahimi and Farzamand 2016). The shear stress influence on NEMS subjected to different load has been discussed by Ebrahimi and Shafiei (2016), Ebrahimi and Farzamand (2016), Ebrahimi and Barati (2017).

Bulge test is an established non-destructive technique for characterizing the mechanical properties of thin film. It has the advantage of being able to characterize the residual stress, elastic modulus, Poisson ratio and other important parameters such as strength and fracture toughness. While at the same time, the sample preparation is relatively simple compared to others mechanical characterization techniques. In the bulge test, a uniform pressure is applied to one side of a free-standing thin film, causing it to deflect toward the other side. The mechanical properties can be obtained from the static pressure 'P' vs. the membrane deflection 'w' relation.

However, the accuracy of results is very sensitive to many sources of errors, like the errors related to the geometry, sample holder, interferometry measurement, pressure measurement and to the analytical model of the load deflection equation. The current work takes into account the above mentioned errors sources in order to analyze and to reduce them for new material are not use in Micro/Nano sensors before that work. Symmetric cross-ply basalt fiber reinforced polymer (BFRP) laminated composite NRTF are tested. This material was chosen because it is a viable and promising alternative to metal materials for their high stiffness and strength to weight ratios, resistance to corrosion, sustainability, and lightweight and improve fatigue resistance and damage tolerance capability, thus it may be useful to investigate this work aims.

2. Bulge test principle

The bulge test consists in measuring the thin film deformation under a differential pressure. The calculation of the relationship between the pressure and the deflection is a difficult problem.

Numerous works to predict the behavior and characteristics of materials under bulging have been undertaken and reported here, the first application of bulge test technique, conducted by (Hill 1950, Mellor 1956) on the bulging of circular diaphragms being the earlier contributions in this field. Chater and Neale (1983) have examined the large strain behavior of a circular membrane under uniform hydrostatic pressure for materials with transversely isotropic plastic properties. They are first applied to derive the governing equations for the pressurized membrane. (Ilahi *et al*. 1981, Ilahi and Paul 1985, Kular and The 1972) have investigated the hydrostatic bulging of anisotropic Aluminum sheets by comparing the experimental results with the theoretical predicted values. Comparison is made with theoretical and experimental results obtained also by other investigators (Brandon *et al*. 1979, Tang 1982, Hill 1990). On the other way of the bulge test research goals in this research decade to obtain the influence of material parameters on the hydrostatic bulging, Zeghloul *et al*. (1991) examined the plastic bulging of pressurized circular membranes with particular attention to the effect of material parameters on the inherent in

homogeneity of the test. Also, Wang and Shammamy (1969) analyzed the hydrostatic bulging of a circular sheet clamped on the basis of both an incremental theory and the corresponding total strain theory of plasticity to show the effects of material types. The material of the sheet is assumed to have strain-hardening capacity and to be anisotropic in the thickness direction. They found that the incremental theory predicts that as the polar strain increases the pressure reaches a maximum and then decreases, whereas the total strain theory gives unsatisfactory results. Altabey (2017) studied the thermo-mechanical behavior of Micro circular diaphragm (MCD) by using bulge test technique. He derived the partial deferential equation of MCD according to diaphragm conditions to establish the analytical solution of bulged MCD for thermo-mechanical characterization with taking in-to account effect of the residual strength from pre-stressed loading. The results show that, the good convergence between the finite element model and analytical model which confirm the successes of he presented technique.

The objective of the theoretical and numerical work to date has been to predict the behavior and characteristics of the metal under the hydrostatic bulging process and to determine the relationships among pressure, strain, and geometrical changes as accurately as possible. Storakers (1966) was being the earlier work used the numerical solution to study the bulge test. He presented an analysis of the plastic deformation including instability phenomena of a circular membrane subject to one-sided hydrostatic pressure. Equations determining stresses and strains are given for the deformation process of materials with a parabolic stress-strain curve. Numerical solutions have been carried out for some special cases. Then several researchers used the numerical solution to save time effort in experimental work and to check validity the results that are come from experimental and theoretical works. Ahmed and Hashmi (1998) studied the effect of combined pressure and in-plane compressive load on the sheet-plate by the finite-element method. The contact condition between the die and the sheet-plate is also taken into consideration in the analysis. Further, the analysis is undertaken also for the pressure-only loading case and the results are compared. Wan *et al*. (2003) measured a tensile residual stress in a plate or membrane clamped at the perimeter by either applying a uniform hydrostatic pressure or a central load via a cylindrical punch (with several different loading configurations). Analytical constitutive relations are derived here based on an average membrane stress approximation and are compared to finite element analysis results. Also in the last decades the numerical solution is playing important side in bulge test technique to determine of the mechanical characteristics of metals.

Since this time, the bulge test technique research was taken the way of investigating the accuracy and reliability to study the mechanical properties of thin film materials, and effects parameters on it to proof the bulge test performance and capabilities as the research work by Itozaki (1982) showed that failure to include the initial height of the membrane in the analysis leads to an apparent nonlinear elastic behavior of the film, then also Small *et al*. (1992) analyzed the influence of initial film conditions such as film wrinkling, residual stress, and initial height of the membrane using finite element analysis. The accuracy and reliability of the bulge test has been analyzed by many investigators (Vlassak 1994, Grolleau *et al*. 2008, Jung *et al*. 2012, 2013, Yang *et al*. 2014, Zhang *et al*. 2015, Huang *et al*. 2016, Suttner and Merklein 2016). These authors point out that the, although the determination of the plane-strain modulus in the light of the plane-strain bulge equation is fairly accurate, the calculation of the residual stress is not satisfied as expected, especially for low residual stress. Finally, some of these work proposed an approach for analyzing bulge test data, which will improve the accuracy and reliability of this bulge test technique.

The plane-strain bulge test is a powerful new technique for measuring the mechanical properties of thin films. In this technique, the stress–strain curve of a thin film is determined from

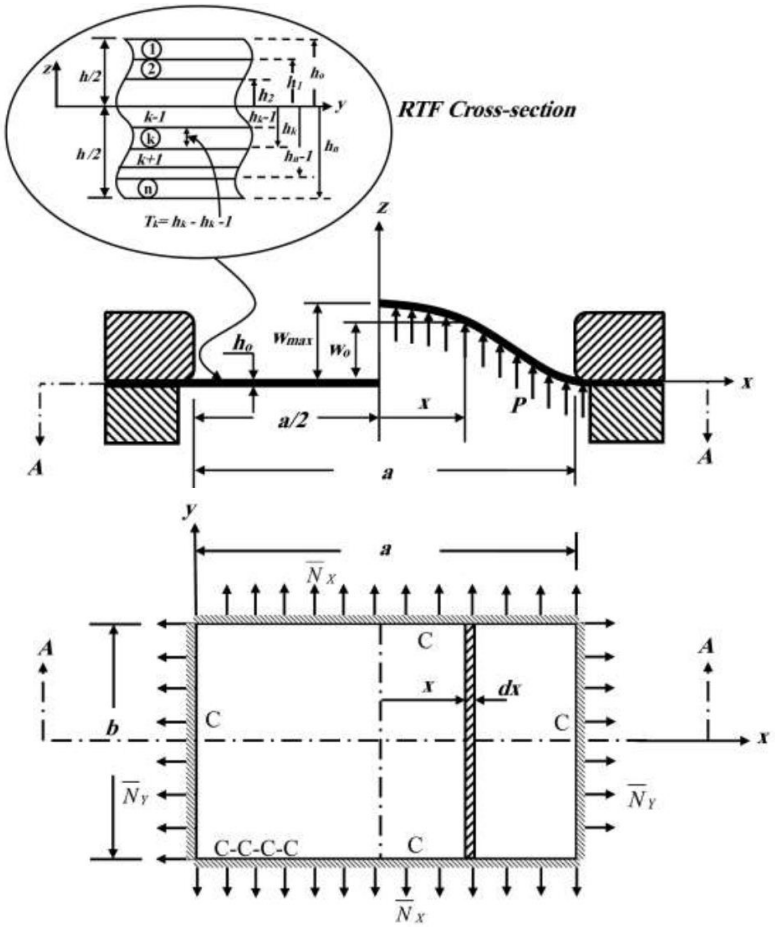

Fig. 1 The geometrical model of bulge test for BFRP composite NRTF subjected to in-plane (pre-stressed) load $\overline{N}_X$ and $\overline{N}_Y$ with clamped edges (CCCC)

the pressure-deflection behavior of the laminated NRTF, as presented in Fig. 1. For a thin film in a state of plane strain, film stress and stain are distributed uniformly across the membrane width, and simple analytical formulae for stress and strain can be established (Xiang *et al*. 2005).

3. The bulge test of NRTF model

3.1 Geometrical model

Fig. 1 represents the geometrical model of BFRP laminated composite NRTF before and after displacement at left half and right half side respectively. As shown in the figure the NRTF has a length at *x*-direction (a) and a length at *y*-direction (b) and the thickness (h_o). The NRTF is first pre-stress under radial stress σ_0 to ensure the initial deflection before applied the load equal zero and then clamped between two plates. The lower side of the film is subjected to a differential pressure (P) to a deformation of the laminated composite NRTF.

The BFRP laminate composite pipe was manufactured using five layers of basalt fibre with

orientation $[0°/90°/0°/90°/0°]_s$ and a polymer resin matrix with a length at x-direction a = 100 nm and a length at y-direction b = 50 nm. The thickness of all plies were 1 nm. The corresponding elastic modulus values were E_1 = 96.74 GPa, $E_2 = E_3$ = 22.55 GPa, and the Shear modulus values were $G_1 = G_3$ = 10.64 Gpa, G_2 = 8.73 GPa. Poisson coefficients were $\upsilon_1 = \upsilon_3$ = 0.3, υ_2 = 0.6 and the density was 2700 kg/m^3.

3.2 Theory and formulation

3.2.1 The governing partial differential equations

A standard x, y, z *coordinate* system, as shown in Fig. 1, is used in deriving the equations. The displacements in the x, y, z *directions* are denoted u_o, v_o, w_o, respectively. The displacements in the x and y directions i.e., u_o and v_o are very small so we can be neglected and the effective equation that is the equation at the direction of the deflection w_o. The governing Partial differential equations of Anisotropic laminated rectangular plates with thickness h subjected to uniform pressure load P on the terms of the plate deflection w_o and in-plane force $\overline{N}_X$, $\overline{N}_Y$ and $\overline{N}_{XY}$ acting in the plane of symmetric cross-ply laminates pre-stressed NRTF are become

$$D_{11}\frac{\partial^4 w_o}{\partial x^4} + 2(D_{12} + 2D_{66})\frac{\partial^4 w_o}{\partial x^2 \partial y^2} + D_{22}\frac{\partial^4 w_o}{\partial y^4} + \overline{N}_X\frac{\partial^2 w_o}{\partial x^2} + \overline{N}_Y\frac{\partial^2 w_o}{\partial y^2} + \rho\frac{\partial^2 w_o}{\partial t^2} = P \tag{1}$$

OR in contraction form

$$D_{11}W_{xxxx} + 2(D_{12} + 2D_{66})W_{xxyy} + D_{22}W_{yyyy} + \overline{N}_X W_{xx} + 2\overline{N}_{XY}W_{xy} + \overline{N}_Y W_{yy} + \rho\, W_{tt} = P \tag{2}$$

Where: $D_{ij} = \frac{1}{3}\frac{h^3(y)}{h_o^3}\sum_{k=1}^{n}\left[(\overline{Q}_{ij})\right]_k (h_{ok}^3 - h_{ok-1}^3), \quad i, j = 1, 2, 3, ...$

For steady state condition $\frac{\partial^2 w_o}{\partial t^2} = 0$, Eq. (2) will take the form:

$$D_{11}W_{xxxx} + 2(D_{12} + 2D_{66})W_{xxyy} + D_{22}W_{yyyy} + \overline{N}_X W_{xx} + 2\overline{N}_{XY}W_{xy} + \overline{N}_Y W_{yy} = P \tag{3}$$

For pre-stressed rectangular thin plate in the hydraulic bulge system the in-plane Load are in x and y direction only i.e., $\overline{N}_{XY} = 0$. Thus, the governing Partial differential Eq. (3) are become

$$D_{11}W_{xxxx} + 2(D_{12} + 2D_{66})W_{xxyy} + D_{22}W_{yyyy} + \overline{N}_X W_{xx} + \overline{N}_Y W_{yy} = P \tag{4}$$

By divided the Eq. (4) by D_{22} and introducing the following constants

$$\psi_1 = \frac{D_{11}}{D_{22}}, \quad \psi_2 = \frac{(D_{12} + 2D_{66})}{D_{22}}, \quad \alpha_1 = \frac{\overline{N}_X}{D_{22}}, \quad \alpha_2 = \frac{\overline{N}_Y}{D_{22}}, \quad \overline{P} = \frac{P}{D_{22}}$$

Eq. (4) will take the form

$$\psi_1 W_{xxxx} + 2\psi_2 W_{xxyy} + W_{yyyy} + \alpha_1 W_{xx} + \alpha_2 W_{yy} = \overline{P} \tag{5}$$

By transfer the right hand side in Eq. (5) to left hand side will take the form

$$\psi_1 W_{xxxx} + 2\psi_2 W_{xxyy} + W_{yyyy} + \alpha_1 W_{xx} + \alpha_2 W_{yy} - \overline{P} = 0 \tag{6}$$

3.2.2 Levy's Method for solution of the governing partial differential equations

Levy suggested the solution of Eq. (6) be expressed in terms of complementary, w_h; and particular, w_p, parts, each of which consists of a single Fourier series where unknown functions are determined from the prescribed boundary conditions. Thus, the solution is expressed as follows

$$w_o = w_h + w_P \tag{7}$$

Consider a plate with opposite edges, $x = 0$ and $x = a$, clamped edges, and two remaining opposite edges, $y = \pm b/2$, which may have arbitrary supports. The boundary conditions on the clamped edges are

$$\begin{aligned} w_o &= 0\big|_{x=0,a}, \quad \frac{\partial w_o}{\partial x} = 0\Big|_{x=0,a} \\ w_o &= 0\big|_{y=\pm\frac{b}{2}}, \quad \frac{\partial w_o}{\partial y} = 0\Big|_{y=\pm\frac{b}{2}} \end{aligned} \tag{8}$$

The complementary solution is taken to be

$$w_h = \sum_{m=1}^{\infty} f_m(y) \sin\left(\frac{m\pi x}{a}\right) \tag{9}$$

Where $f_m(y)$ is a function of y only; w_h also satisfies the clamped edges boundary conditions Eq. (8). Substituting Eq. (9) into Eq. (6) and according to the obtained values of the characteristic exponents, the solution of the homogeneous equation can be expressed in terms of either exponential function

$$f_m(y) = A'_m e^{m\pi y/a} + B'_m e^{-m\pi y/a} + \frac{m\pi y}{a}\left(C'_m e^{m\pi y/a} + D'_m e^{-m\pi y/a}\right) \tag{10}$$

Or in hyperbolic functions

$$f_m(y) = A_m \sinh\left(\frac{m\pi y}{a}\right) + B_m \cosh\left(\frac{m\pi y}{a}\right) + \frac{m\pi y}{a}\left(C_m \sinh\left(\frac{m\pi y}{a}\right) + D_m \cosh\left(\frac{m\pi y}{a}\right)\right) \tag{11}$$

The second form, Eq. (11), is more convenient for calculations. The complementary solution given by Eq. (9) becomes

$$w_h = \sum_{m=1}^{\infty}\left[A_m \sinh\left(\frac{m\pi y}{a}\right) + B_m \cosh\left(\frac{m\pi y}{a}\right) + \frac{m\pi y}{a}\left(C_m \sinh\left(\frac{m\pi y}{a}\right) + D_m \cosh\left(\frac{m\pi y}{a}\right)\right)\right] \sin\left(\frac{m\pi x}{a}\right) \tag{12}$$

Where the constants A_m, B_m, C_m and D_m are obtained from the boundary conditions on the edges $y = \pm b/2$.

The particular solution, w_P, in Eq. (7), can also be expressed in a single Fourier series as

$$w_P(x,y)=\sum_{m=1}^{\infty} g_m(y)\sin\left(\frac{m\pi x}{a}\right) \tag{13}$$

The pressure (lateral distributed) load $P(x, y)$ is taken to be the following

$$P(x,y)=\sum_{m=1}^{\infty} P_m(y)\sin\left(\frac{m\pi x}{a}\right), \tag{14}$$

Where $P_m(y)$ represent coefficients to be determined. It can be easily verified that the expression for particular deflections Eq. (13) automatically satisfies the prescribed boundary conditions Eq. (8).

By Substituting Eqs. (13) and (14) into Eq. (6), and after some derivatives the particular solution is of the following form

$$\therefore w_P(x,y)=\frac{4\bar{P}a^4}{\pi^5}\sum_{m=1,3,5,\cdots}^{\infty}\frac{\pi^2}{\left(\psi_1\pi^2m^5-\alpha_1m^3a^2\right)}\sin\left(\frac{m\pi x}{a}\right) \tag{15}$$

Combining Eqs. (15) and (12), we obtain

$$\begin{aligned} w_o=\sum_{m=1,3,5,\cdots}^{\infty}\Bigg[& A_m\sinh\left(\frac{m\pi y}{a}\right)+B_m\cosh\left(\frac{m\pi y}{a}\right)+\frac{m\pi y}{a}\left(C_m\sinh\left(\frac{m\pi y}{a}\right)\right. \\ & \left.+D_m\cosh\left(\frac{m\pi y}{a}\right)\right)+\frac{4\bar{P}a^4}{\pi^3\left(\psi_1\pi^2m^5-\alpha_1m^3a^2\right)}\Bigg]\sin\left(\frac{m\pi x}{a}\right) \end{aligned} \tag{16}$$

Due to the symmetry of the boundary conditions and applied loading, we can conclude that the plate deflection will be also symmetrical about the *x axis*, i.e., $w_o(x, y) = w_o(x, -y)$. This condition is satisfied by Eq. (12) if we let $A_m = D_m = 0$. Then, combining Eqs. (12) and (15), we obtain

$$w_o=\sum_{m=1,3,5,\cdots}^{\infty}\left[B_m\cosh\left(\frac{m\pi y}{a}\right)+C_m\frac{m\pi y}{a}\sinh\left(\frac{m\pi y}{a}\right)+\frac{4\bar{P}a^4}{\pi^3\left(\psi_1\pi^2m^5-\alpha_1m^3a^2\right)}\right]\sin\left(\frac{m\pi x}{a}\right) \tag{17}$$

Where the constants B_m and C_m are obtained from the boundary conditions on the edges at $y = \pm b/2$.

Eq. (17) exactly satisfy Eq. (6) and the boundary conditions (8) at $x = 0$ and $x = a$. The remaining boundary conditions are, as follows

$$w_o=0\Big|_{\pm b/2},\quad \frac{\partial w_o}{\partial y}=0\Big|_{\pm b/2}$$

We can obtain the constants A_m, B_m, C_m and D_m exactly satisfy Eq. (17) and the boundary conditions of clamped edges are

$$A_m = 0, \qquad B_m = -\gamma_m \left[\left(\frac{\phi_m \tanh^2(\phi_m)}{(\phi_m \cosh(\phi_m) + \sinh(\phi_m) - \phi_m \tanh(\phi_m)\sinh(\phi_m))} \right) + \frac{1}{\cosh(\phi_m)} \right],$$

$$C_m = \frac{\gamma_m \tanh(\phi_m)}{(\phi_m \cosh(\phi_m) + \sinh(\phi_m) - \phi_m \tanh(\phi_m)\sinh(\phi_m))}, \qquad D_m = 0.$$

Where: $\phi_m = \dfrac{m\pi b}{2a}$, $\gamma_m = \dfrac{4\bar{P}a^4}{\pi^3(\psi_1 \pi^2 m^5 - \alpha_1 m^3 a^2)}$

The deflection of the plate surface, Eq. (17), may thus be expressed

$$w_o = \sum_{m=1,3,5,\cdots}^{\infty} \gamma_m \left[\left(\frac{-\phi_m \tanh^2(\phi_m)}{(\phi_m \cosh(\phi_m) + \sinh(\phi_m) - \phi_m \tanh(\phi_m)\sinh(\phi_m)))} - \frac{1}{\cosh(\phi_m)} \right) \cosh\left(\frac{2\phi_m y}{b} \right) + \left(\frac{\tanh(\phi_m)}{(\phi_m \cosh(\phi_m) + \sinh(\phi_m) - \phi_m \tanh(\phi_m)\sinh(\phi_m)))} \right) \left(\frac{2\phi_m y}{b} \right) \sinh\left(\frac{2\phi_m y}{b} \right) + 1 \right] \sin\left(\frac{m\pi x}{a} \right) \tag{18}$$

The maximum deflection is obtained at the film center (x= a/2 and y = 0), where

$$w_{\max} = \sum_{m=1,3,5,\cdots}^{\infty} \gamma_m (-1)^{\frac{m-1}{2}} \left[\left(\frac{-\phi_m \tanh^2(\phi_m)}{(\phi_m \cosh(\phi_m) + \sinh(\phi_m) - \phi_m \tanh(\phi_m)\sinh(\phi_m)))} - \frac{1}{\cosh(\phi_m)} \right) + 1 \right] \tag{19}$$

3.2.3 laminated NRTF moments and shear force

Considering an elemental parallelepiped cut out of the film, as shown in Fig. 2, we assign positive internal forces and moments to the near faces of the film element. To satisfy the equilibrium of the element, negative internal forces and moments must act on its far sides. The first subscript of the internal forces refers to the direction of the surface normal pertinent to the section on which the force acts. The subscripts of the internal bending and of the twisting moments refer to the stresses of which they are produced.

After equilibrium of the film element for internal forces and moments and after some deriving on this equilibrium, we can obtain the total equivalent shear forces and moments applied to the middle surface in terms of displacements, which are known as the stress resultants and stress couples. The stress resultants and stress couples are referred to as the shear forces, Q_x and Q_y, as well as the bending and twisting moments M_x, M_y, and M_{xy}, respectively.

The bending moments and the shear force in terms of displacements for symmetric cross-ply laminate NRTF are given by

$$\left.\begin{aligned} M_X &= -D_{11} \frac{\partial^2 w_o}{\partial x^2} - D_{12} \frac{\partial^2 w_o}{\partial y^2} \\ M_Y &= -D_{12} \frac{\partial^2 w_o}{\partial x^2} - D_{22} \frac{\partial^2 w_o}{\partial y^2} \\ M_{XY} &= -2D_{66} \frac{\partial^2 w_o}{\partial x \partial y} \end{aligned}\right\} \tag{20}$$

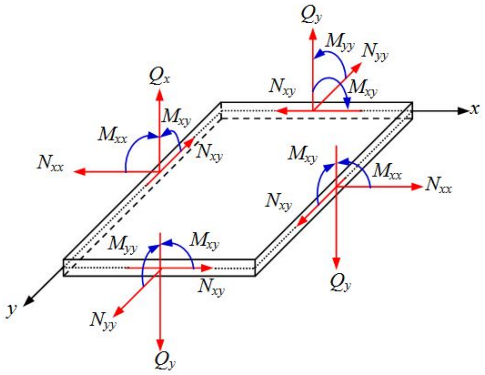

Fig. 2 The shear forces and moments on a laminate

$$\left.\begin{aligned} Q_X &= -D_{11}\frac{\partial^3 w_o}{\partial x^3} - (D_{12}+4D_{66})\frac{\partial^3 w_o}{\partial x \partial y^2} \\ Q_Y &= -D_{22}\frac{\partial^3 w_o}{\partial y^3} - (D_{12}+4D_{66})\frac{\partial^2 w_o}{\partial x^2 \partial y} \end{aligned}\right\} \tag{21}$$

Referring to Fig. 2, we can express the bending and twisting moments, as well as the shear forces, in terms of the stress components, i.e.

$$\begin{bmatrix} M_X \\ M_Y \\ M_{XY} \end{bmatrix} = \int_{-\frac{h}{2}}^{\frac{h}{2}} \begin{bmatrix} \sigma_X \\ \sigma_Y \\ \tau_{XY} \end{bmatrix} z \, dz \tag{22}$$

$$\begin{bmatrix} Q_X \\ Q_Y \end{bmatrix} = \int_{-\frac{h}{2}}^{\frac{h}{2}} \begin{bmatrix} \tau_{XZ} \\ \tau_{YZ} \end{bmatrix} dz \tag{23}$$

3.2.4 laminated NRTF stress-strain relations

Similarly, the formulas for the plane stress components, from Eq. (22) are written in the following form

$$\sigma_X = \frac{12M_X}{h^3}Z, \quad \sigma_X = \frac{12M_Y}{h^3}Z, \quad \tau_{XY} = \frac{12M_{XY}}{h^3}Z \tag{24}$$

Where M_X, M_Y and M_{XY} are determined by Eqs. (20), clearly the maximum stresses take place on the surfaces $Z = \pm h/2$ of the thin film.

The stress-strain relations for symmetric cross-ply laminate NRTF are given by

$$\begin{bmatrix} \sigma_X \\ \sigma_Y \\ \tau_{XY} \end{bmatrix} = \left[\overline{Q}\right] \begin{bmatrix} \varepsilon_X \\ \varepsilon_Y \\ \gamma_{XY} \end{bmatrix} \tag{25}$$

Where: $\left[\overline{Q}\right] = [T_1][Q][T_2]^{-1}$ and $Q_{ij} = \begin{bmatrix} Q_{11} & Q_{12} & Q_{13} \\ Q_{12} & Q_{22} & Q_{23} \\ Q_{13} & Q_{23} & Q_{66} \end{bmatrix} = \begin{bmatrix} \frac{E_{11}}{(1-\upsilon_{12}\upsilon_{21})} & \frac{\upsilon_{21}E_{11}}{(1-\upsilon_{12}\upsilon_{21})} & 0 \\ \frac{\upsilon_{21}E_{11}}{(1-\upsilon_{12}\upsilon_{21})} & \frac{E_{22}}{(1-\upsilon_{21}\upsilon_{12})} & 0 \\ 0 & 0 & G_{12} \end{bmatrix}$,

$[T_1]=[T]=\begin{bmatrix} \cos^2\theta & \sin^2\theta & 2\sin\theta\cos\theta \\ \sin^2\theta & \cos^2\theta & -2\sin\theta\cos\theta \\ -\sin\theta\cos\theta & \sin\theta\cos\theta & \cos^2\theta-\sin^2\theta \end{bmatrix}$ is the transformation matrix,

$T_2 = [T]^{-1}[R]\,[R]^{-1} = \begin{bmatrix} \cos^2\theta & \sin^2\theta & -\sin\theta\cos\theta \\ \sin^2\theta & \cos^2\theta & \sin\theta\cos\theta \\ 2\sin\theta\cos\theta & -2\sin\theta\cos\theta & \cos^2\theta-\sin^2\theta \end{bmatrix}$, $[R]=\begin{bmatrix} 1 & 0 & 0 \\ 0 & 1 & 0 \\ 0 & 0 & 2 \end{bmatrix}$ is the simple matrix.

Since the strain relations of NRHF are given by

$$\varepsilon_X = -z\frac{\partial^2 w_o}{\partial x^2}, \quad \varepsilon_Y = -z\frac{\partial^2 w_o}{\partial y^2}, \quad \gamma_{XY} = -2z\frac{\partial^2 w_o}{\partial x \partial y} \tag{26}$$

For the bending moment M_x, M_y and M_{xy} substituting Eqs. (18) and (20) may thus be expressed

$$M_X = \sum_{m=1,3,5,\cdots}^{\infty}\left[B_m\left(D_{11}\left(\frac{m\pi}{a}\right)^2 - D_{12}\left(\frac{2\phi_m}{b}\right)^2\right)\cosh\left(\frac{2\phi_m y}{b}\right) + D_{11}\left(\frac{m\pi}{a}\right)^2\gamma_m + C_m\left(D_{11}\left(\frac{m\pi}{a}\right)^2 - D_{12}\left(\frac{2\phi_m}{b}\right)^2\right)\left(\frac{2\phi_m y}{b}\right)\sinh\left(\frac{2\phi_m y}{b}\right) - 2C_m D_{12}\left(\frac{2\phi_m}{b}\right)^2\cosh\left(\frac{2\phi_m y}{b}\right)\right]\sin\left(\frac{m\pi x}{a}\right) \tag{27}$$

$$M_Y = \sum_{m=1,3,5,\cdots}^{\infty}\left[B_m\left(D_{12}\left(\frac{m\pi}{a}\right)^2 - D_{22}\left(\frac{2\phi_m}{b}\right)^2\right)\cosh\left(\frac{2\phi_m y}{b}\right) + D_{12}\left(\frac{m\pi}{a}\right)^2 + C_m\left(D_{12}\left(\frac{m\pi}{a}\right)^2 - D_{22}\left(\frac{2\phi_m}{b}\right)^2\right)\left(\frac{2\phi_m y}{b}\right)\sinh\left(\frac{2\phi_m y}{b}\right) - 2C_m D_{22}\left(\frac{2\phi_m}{b}\right)^2\cosh\left(\frac{2\phi_m y}{b}\right)\right]\sin\left(\frac{m\pi x}{a}\right) \tag{28}$$

$$M_{XY} = \sum_{m=1,3,5,\cdots}^{\infty} D_{66}\frac{m\pi}{a}\frac{4\phi_m}{b}\left[-B_m\sinh\left(\frac{2\phi_m y}{b}\right) - C_m\left(\left(\frac{2\phi_m y}{b}\right)\cosh\left(\frac{2\phi_m y}{b}\right) + \sinh\left(\frac{2\phi_m y}{b}\right)\right)\right]\cos\left(\frac{m\pi x}{a}\right) \tag{29}$$

For shear force Q_x and Q_y substituting Eqs. (18) and (21) may thus be expressed

$$\therefore Q_X = \sum_{m=1,3,5,\cdots}^{\infty}\Bigg[B_m\frac{m\pi}{a}\left(D_{11}\left(\frac{m\pi}{a}\right)^2-(D_{12}+4D_{66})\left(\frac{2\phi_m}{b}\right)^2\right)\cosh\left(\frac{2\phi_m y}{b}\right)$$
$$C_m\frac{m\pi}{a}\left(D_{11}\left(\frac{m\pi}{a}\right)^2-(D_{12}+4D_{66})\left(\frac{2\phi_m}{b}\right)^2\right)\left(\frac{2\phi_m y}{b}\right)\sinh\left(\frac{2\phi_m y}{b}\right)+D_{11}\left(\frac{m\pi}{a}\right)^3\gamma_m \quad (30)$$
$$-2C_m(D_{12}+4D_{66})\frac{m\pi}{a}\left(\frac{2\phi_m}{b}\right)^2\cosh\left(\frac{2\phi_m y}{b}\right)\Bigg]\cos\left(\frac{m\pi x}{a}\right)$$

$$\therefore Q_Y = \sum_{m=1,3,5,\cdots}^{\infty}\Bigg[B_m\frac{2\phi_m}{b}\left((D_{12}+4D_{66})\left(\frac{m\pi}{a}\right)^2-D_{22}\left(\frac{2\phi_m}{b}\right)^2\right)\sinh\left(\frac{2\phi_m y}{b}\right)$$
$$+C_m\frac{2\phi_m}{b}\left((D_{12}+4D_{66})\left(\frac{m\pi}{a}\right)^2-D_{22}\left(\frac{2\phi_m}{b}\right)^2\right)\left(\frac{2\phi_m y}{b}\right)\cosh\left(\frac{2\phi_m y}{b}\right) \quad (31)$$
$$C_m\left((D_{12}+4D_{66})\left(\frac{m\pi}{a}\right)^2\frac{2\phi_m}{b}-3D_{22}\left(\frac{2\phi_m}{b}\right)^3\right)\sinh\left(\frac{2\phi_m y}{b}\right)\Bigg]\sin\left(\frac{m\pi x}{a}\right)$$

Substituting the Eqs. (27), (28) and (29) into Eq. (24), we obtain the following expressions for the plane stress components similarly, the formulas for the plane stress components, from Eq. (24) are written in the following form

$$\sigma_X=\frac{12M_X}{h^3}Z,\quad \sigma_X=\frac{12M_Y}{h^3}Z,\quad \tau_{XY}=\frac{12M_{XY}}{h^3}Z$$

Where M_x, M_y and M_{xy} are determined by Eqs. (20). Clearly the maximum stresses take place on the surfaces $Z=\pm h/2$, the stress σ_x, σ_y and τ_{xy} may thus be expressed

$$\sigma_X=\sum_{m=1,3,5,\cdots}^{\infty}\frac{12}{h^3}Z\Bigg[B_m\left(D_{12}\left(\frac{m\pi}{a}\right)^2-D_{22}\left(\frac{2\phi_m}{b}\right)^2\right)\cosh\left(\frac{2\phi_m y}{b}\right)+D_{12}\left(\frac{m\pi}{a}\right)^2+C_m\left(D_{12}\left(\frac{m\pi}{a}\right)^2$$
$$-D_{22}\left(\frac{2\phi_m}{b}\right)^2\right)\left(\frac{2\phi_m y}{b}\right)\sinh\left(\frac{2\phi_m y}{b}\right)-2C_m D_{22}\left(\frac{2\phi_m}{b}\right)^2\cosh\left(\frac{2\phi_m y}{b}\right)\Bigg]\sin\left(\frac{m\pi x}{a}\right) \quad (32)$$

$$\sigma_Y=\sum_{m=1,3,5,\cdots}^{\infty}\frac{12}{h^3}Z\Bigg[B_m\left(D_{12}\left(\frac{m\pi}{a}\right)^2-D_{22}\left(\frac{2\phi_m}{b}\right)^2\right)\cosh\left(\frac{2\phi_m y}{b}\right)+D_{12}\left(\frac{m\pi}{a}\right)^2+C_m\left(D_{12}\left(\frac{m\pi}{a}\right)^2$$
$$-D_{22}\left(\frac{2\phi_m}{b}\right)^2\right)\left(\frac{2\phi_m y}{b}\right)\sinh\left(\frac{2\phi_m y}{b}\right)-2C_m D_{22}\left(\frac{2\phi_m}{b}\right)^2\cosh\left(\frac{2\phi_m y}{b}\right)\Bigg]\sin\left(\frac{m\pi x}{a}\right) \quad (33)$$

$$\tau_{XY}=\sum_{m=1,3,5,\cdots}^{\infty}\frac{12}{h^3}ZD_{66}\frac{m\pi}{a}\frac{4\phi_m}{b}\left[-B_m\sinh\left(\frac{2\phi_m y}{b}\right)\right. \quad (34)$$

$$-C_m\left(\left(\frac{2\phi_m y}{b}\right)\cosh\left(\frac{2\phi_m y}{b}\right)+\sinh\left(\frac{2\phi_m y}{b}\right)\right)\Bigg]\cos\left(\frac{m\pi x}{a}\right) \tag{34}$$

For the strain ε_x, ε_y and γ_{xy} substituting Eqs. (18) and (26) may thus be expressed

$$\varepsilon_X=-z\left(\frac{m\pi}{a}\right)^2\left[-B_m\cosh\left(\frac{2\phi_m y}{b}\right)-C_m\left(\frac{2\phi_m y}{b}\right)\sinh\left(\frac{2\phi_m y}{b}\right)-\gamma_m\right]\sin\left(\frac{m\pi x}{a}\right) \tag{35}$$

$$\varepsilon_Y=-z\left(\frac{2\phi_m}{b}\right)^2\left[B_m\cosh\left(\frac{2\phi_m y}{b}\right)+C_m\left(\left(\frac{2\phi_m y}{b}\right)\sinh\left(\frac{2\phi_m y}{b}\right)+2\cosh\left(\frac{2\phi_m y}{b}\right)\right)\right]\sin\left(\frac{m\pi x}{a}\right) \tag{36}$$

$$\gamma_{XY}=-z\frac{4m\pi\phi_m}{ab}\left[B_m\sinh\left(\frac{2\phi_m y}{b}\right)+C_m\left(\left(\frac{2\phi_m y}{b}\right)\cosh\left(\frac{2\phi_m y}{b}\right)+\sinh\left(\frac{2\phi_m y}{b}\right)\right)\right]\cos\left(\frac{m\pi x}{a}\right) \tag{37}$$

3.2.5 The laminate NRTF thickness distribution

The membrane theory is commonly used to determine the flow stress curve with the bulge test (Panknin 1959, Gologranc 1975), Fig. 3. The membrane theory neglects bending stresses across the film thickness. Thus, it is only applicable for thin film and gives for the bulge test the following relationship between stresses, strain and film geometry. Let as consider free forming of a laminated thin film. The current half arc length of any meridian passing through the dome apex is equal to $R\alpha$ where R is the dome radius and α is half the angle subtended by the dome surface at the center of curvature, see Fig. 3. Since the initial half arc length of the meridian under consideration equals to the length a, it is stretched $2R\alpha/\alpha = \alpha/\sin\alpha$ times. Proceeding from symmetry, it follows that the principal positive strains are equal to each other and thickness at the dome apex equals.

$$h_d=h_0\left(\frac{\sin\alpha}{\alpha}\right)^2 \tag{38}$$

Since the clamp does not deform during forming, the circumferential deformation along the periphery is negligible. On the other hand, meridian approaching the periphery is stretched by $\alpha/\sin\alpha$ times, and from this it follows that dome thickness at the periphery equals to

$$h_P=h_0\left(\frac{\sin\alpha}{\alpha}\right) \tag{39}$$

At some moment of deformation the point M transfer to point M', and point O to O' as shown in Fig. 3. Let Ψ be the angle between the symmetry axis and the dome radius to the point M' under consideration. The latitude passing the point M' is stretched by x/x_0 times and the dome thickness at the point M' may be found as follow

$$h=h_0\left(\frac{x}{x_0}\right)\left(\frac{\sin\alpha}{\alpha}\right) \tag{40}$$

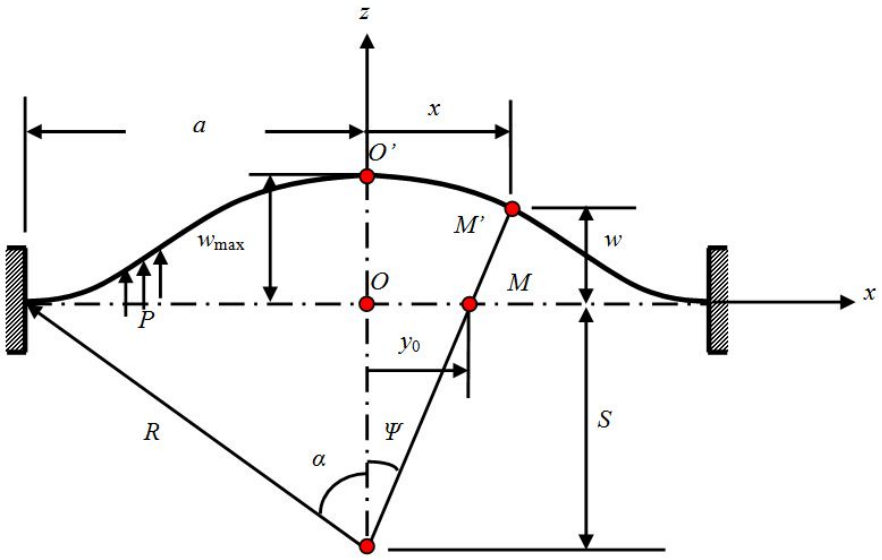

Fig. 3 Schematic of deformation modeling

Taking into account that $x = R \sin\Psi$, $x_0 = ca/2$ and $\Psi = c\alpha$ the dome thickness at any point could be calculated from the following Eq. (39)

$$h = h_0\left(\frac{\Psi}{\sin\Psi}\right)\left(\frac{\sin\alpha}{\alpha}\right)^2 \tag{41}$$

The radius of curvature, see Fig. 3, is

$$R = \frac{a^2 + w_{max}}{2w_{max}}, \quad \alpha = \sin^{-1}\left(\frac{a}{R}\right), \quad \Psi = \tan^{-1}\left(\frac{x}{S}\right) \quad \text{and} \quad S = \frac{a}{\tan\alpha}$$

The dome thickness at any point could be calculated from the following Eq. (41) as a function of (a, w_{max}, h_0, x)

$$\frac{h}{h_0} = \left(\frac{\mu_1}{\mu_2}\right)^2\left(\frac{\mu_3}{\mu_4}\right) \tag{42}$$

Where: $\mu_1 = \frac{2aw_{max}}{(a^2 + w_{max})}$, $\mu_2 = \sin^{-1}(\mu_1)$, $\mu_3 = \tan^{-1}\left(\frac{x}{a}\tan(\mu_2)\right)$, $\mu_4 = \sin(\mu_3)$

4. Results and discussion

The results of the Nano rectangular thin film (NRTF) were used to calculate the mechanical behavior of the NEMS material. In Figs. 4-7 a typical Nano-deformation (deflection and strain) of a NRTF is depicted. The characterized sample is a NRTF made of basalt fiber reinforced polymer (BFRP) laminate composite materials with $[0°/90°/0°/90°/0°]_s$ laminate layer angle, longitudinal

distance is 100 nm, and lateral distance is 50 nm and 5 nm thick.

4.1 Convergence study and accuracy

In this subsection, a convergence investigation is carried out for the proposed method, the residual stress σ_0 and Young's modulus are calculated using presented technique and compared with available results in literatures. Table 1 presents a convergence and comparison study for Si_3N_4 thin films. Silicon nitride (Si_3N_4) is a widely used functional material in MEMS devices due to its superior chemical and mechanical properties.

The computational results which are compared with values available from literatures (Tabata *et al*. 1989, Vlassak and Nix 1992, Edwards *et al*. 2004). A very close agreement is observed.

4.2 BFRP Nano rectangular thin film (*NRTF*)

As shown in the Fig. 4 the transverse Nano-deflection w_o is increased with increased of the NRTF longitudinal distance (a); along *x-direction* and decreased with increased of the NRTF lateral distance (b) along *y-direction* and the maximum Nano-deflection (w_{max} = 7.0527 nm) was occured at pressure 10 Pa at the center of the NRTF at $a = a/2$ and $b = 0$.

Table 1 Convergence study of the residual stress σ_0 and Young's modulus of the Si_3N_4 thin films

	Tabata *et al*. (1989)	Present	Vlassak and Nix (1992)	Present	Edwards *et al*. (2004)	Present
Residual stress σ_0	1 GPa	0.965 GPa	150 MPa	147.82 MPa	130 MPa	127.78 MPa
Young's modulus	290 GPa	287.8 GPa	222 GPa	221 GPa	258 GPa	255.6 GPa

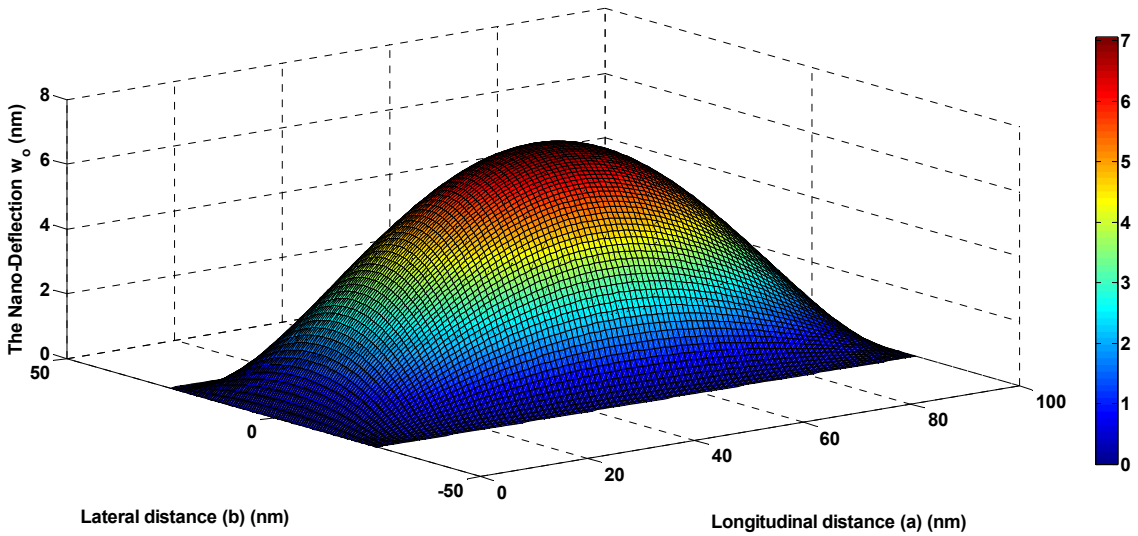

Fig. 4 The 3D Nano-deflection distribution along NRTF for BFRP composite material with $[0°/90°/0°/\ 90°/0°]_s$ laminate layer angle

As shown in the Figs. 5-7 the Nano-strain of ε_x, ε_y and γ_{xy} (nm/nm) distributions are symmetric along longitudinal and lateral directions, so the strain distribution behaviour in quarter of NRTF is the symmetric with corresponding quarter along NRTF axis with the maximum Nano-strain of ε_x, ε_y and γ_{xy} are 0.43504, 0.53257 and 0.38729 (nm/nm) respectively, were occured at pressure 10 Pa. In Fig. 5, the Nano-strain ε_x is increased with increased of the NRTF longitudinal distance (a) along x-direction and decreased with increased of the NRTF lateral distance (b) along y-direction and the maximum Nano-strain ε_x is occured at the center of the NRTF at $a = a/2$ and $b = 0$.

But in Fig. 6, the Nano-strain ε_y is equal zero (nm/nm) for all the NRTF surface except the film ends, where, the Nano-strain ε_y is increased with increased of the NRTF longitudinal distance (a) along x-direction at both ends and the maximum Nano-strain ε_y is occured at the center of the

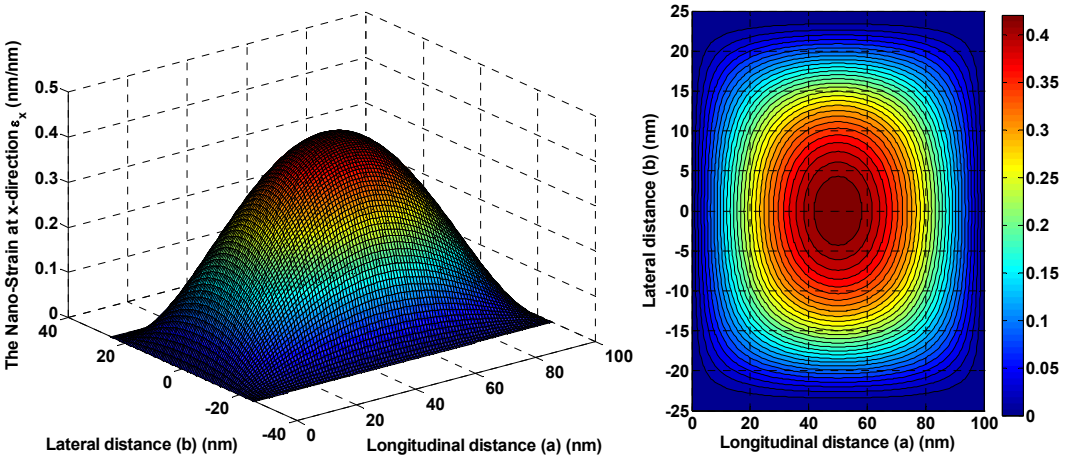

Fig. 5 Nano-strain ε_x (nm/nm) distribution along NRTF for BFRP composite material with $[0°/90°/0°/90°/0°]_s$ laminate layer angle, contour profile at right and 3D profile at left

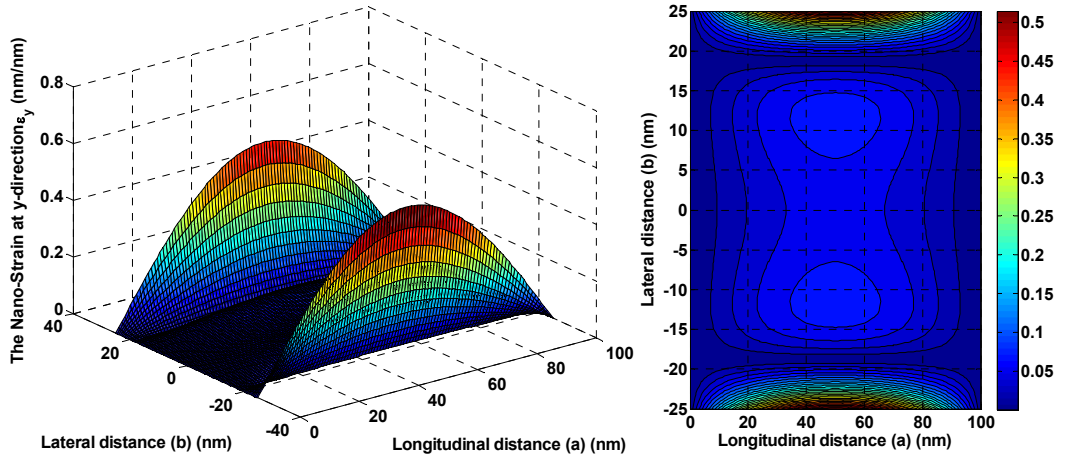

Fig. 6 Nano- strain ε_y (nm/nm) distribution along NRTF for BFRP composite material with $[0°/90°/0°/90°/0°]_s$ laminate layer angle, contour profile at right and 3D profile at left

NRTF edge at $a = a/2$ and $b = \pm b/2$. But the Nano-strain ε_y is equal zero (nm/nm) at other edges of NRTF along y-direction.

In Fig. 7, the Nano-strain γ_{xy} is equal zero (nm/nm) at the center of the NRTF at $a=a/2$ and $b = 0$, the Nano-strain γ_{xy} is decreased from maximum to zero (nm/nm) with increased of the NRTF longitudinal distance (a) along x-direction at $a = a/2$, then increased to maximum, but the Nano-strain γ_{xy} is increased from zero (nm/nm) to maximum with increased of the NRTF lateral distance (b) along y-direction, then decreased to zero. The maximum Nano-strain γ_{xy} is occured almost at four edges of the NRTF at $a = 0$, a and $b = \pm b/4$.

The stress distribution across NRTF thickness in contour profile is illustrated in Fig. 8. As shown in the figure, the stress distribution across NRTF thickness is symmetric above and below the midplane, above midplane is subjected to tension stress and below midplane is subjected to compression stress with the same value of maximum stress ±3.637 pa was occured at pressure 10 Pa and the stress equal zero on the midplane.

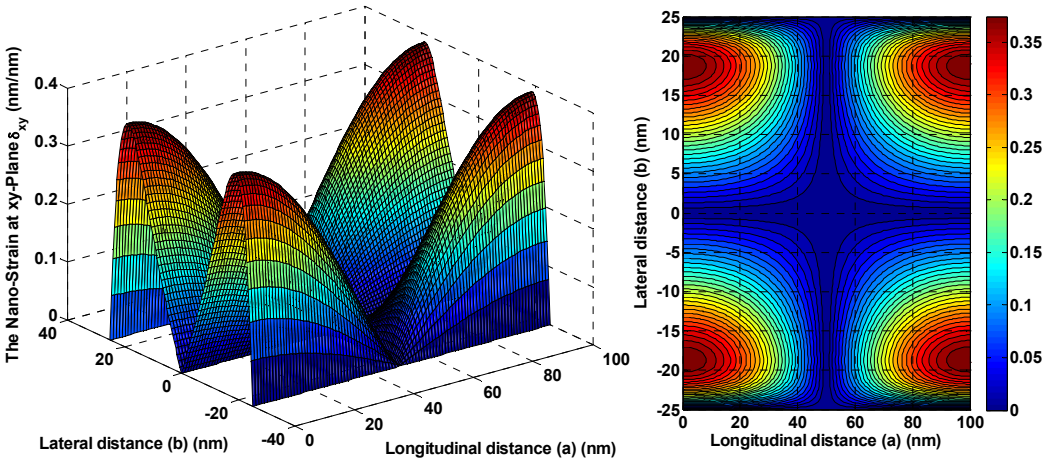

Fig. 7 Nano-strain δ_{xy} (nm/nm) distribution along NRTF for BFRP composite material with $[0°/90°/0°/90°/0°]_s$ laminate layer angle, contour profile at right and 3D profile at left

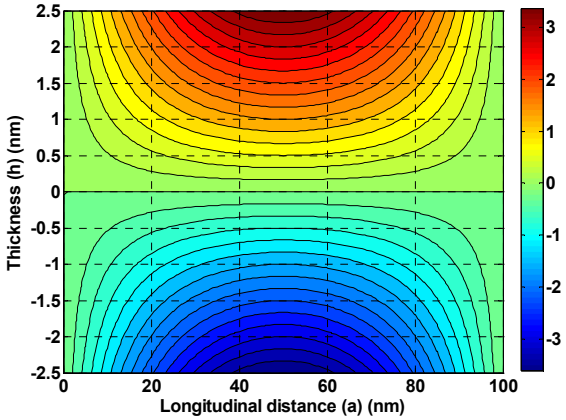

Fig. 8 The stress distribution across NRTF thickness in contour profile

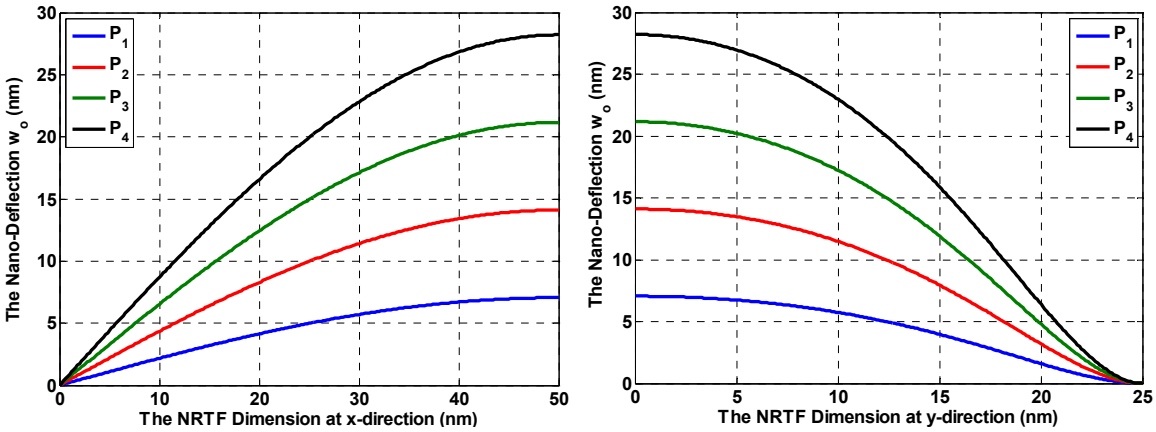

(a) Longitudinal distance (b) Lateral distance

Fig. 9 Nano-Deflection profile with differential pressure of NRTF for BFRP composite material with $[0°/90°/0°/90°/0°]_s$ laminate layer angle

In Fig. 9, differential pressure has been varied between 10 and 25 Pa with a regular step of 5 Pa. This corresponds to measuring transverse Nano-deflection w_o. As shown in the figure, the transverse Nano-deflection wo is increased with increased of the pressure (P) and maximume Nano-deflection $w_{\max}$ varied between 7.0527 and 28.21 nm respectively.

Figs. 10 and 11 show the relationship between stress and Namo-strain of NRTF with differential pressure has been varied between 10 and 25 Pa with a regular step of 5 Pa.

From Figs. 10 and 11 we can see, the Nano-strain is increased with stress and increased of the pressure (P) and maximume Nano-strain varied between 0.43504 and 1.74 (nm/nm) and between 0.06177 and 0.2465 (nm/nm) for ε_x and ε_y respectively. This relation is very important in

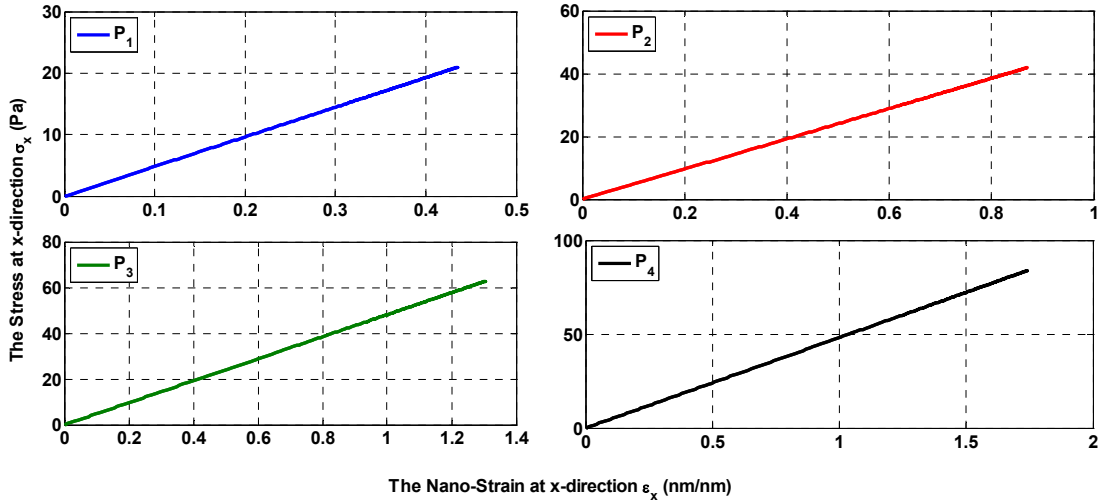

Fig. 10 Stress and Namo-strain relationship at x-direction with differential pressure of NRTF for BFRP composite material with $[0°/90°/0°/90°/0°]_s$ laminate layer angle

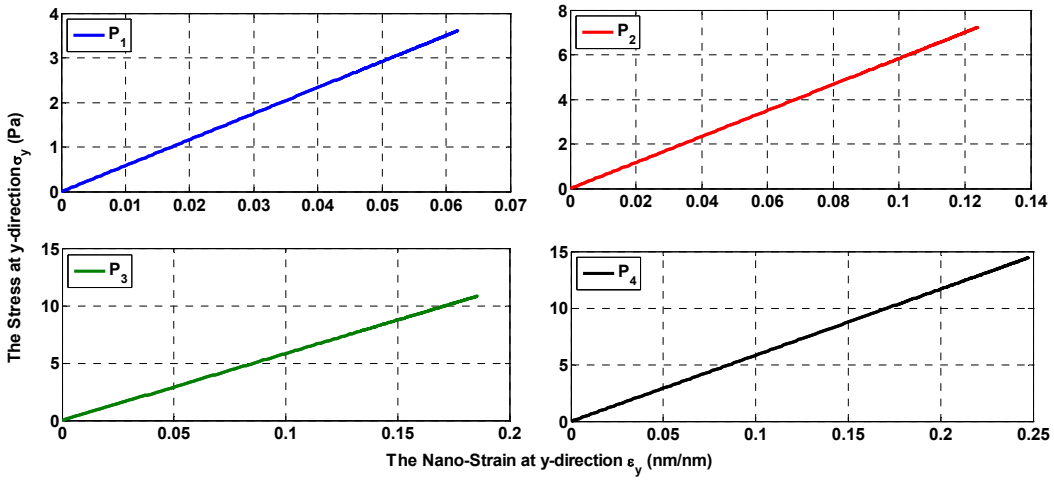

Fig. 11 Stress and Namo-strain relationship at *y-direction* with differential pressure of NRTF for BFRP composite material with $[0°/90°/0°/90°/0°]_s$ laminate layer angle

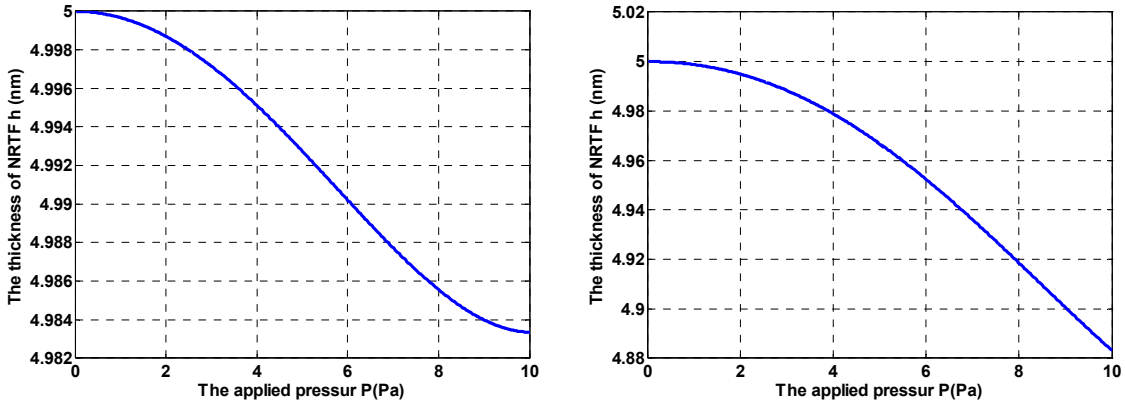

(a) *P* vs. *h* at *x*-direction

(b) *P* vs. *h* at *y*-direction

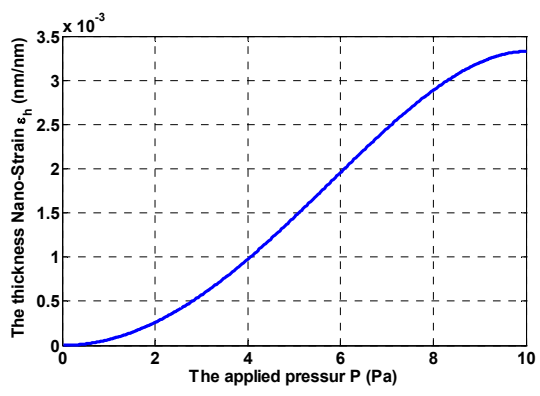

(c) P vs. ε_h at *x*-direction

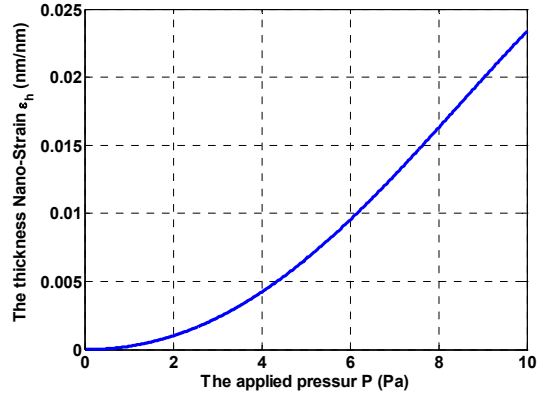

(d) *P* vs. ε_h at *y*-direction

Fig. 12 The relation between differential pressure (P) and Thickness Nano-deformation of NRTF for BFRP composite material with $[0°/90°/0°/90°/0°]_s$ laminate layer angle

engineering analysis where the Young's modulus E of the NRTF material from the slop of this liner relation. As a result, the Young's modulus E can be expressed by $E = \Delta E = \Delta\sigma/\Delta\varepsilon$, and Young's modulus E_x and E_y were calculated 42.01 and 58.63 Gpa respectively.

The Nano-thickness deformation behavior across the NRTF is very important to improve the mechanical behaviour of NRTF, in order to satisfy the film durability for bulging load, therefore, the NEMS reliability.

Fig. 12 shows the Nano-thickness deformation behavior under pressure variations, as shown in the figure the the Nano-thickness (h) is decreased from 5 to 4.883 nm with increased of the applied pressure (P) from 0 to 10 Pa at both directions. While, the thickness Nano-strain (ε_h) is increased with increased of the applied pressure (P) at both directions.

5. Conclusions

In this work the bulging tests is used to study the mechanical properties of Nano rectangular thin film (NRTF) embedded in Nano Electro Mechanical Systems (NEMS), made of basalt fiber reinforced polymer (BFRP) laminate composite materials. These Nano-film are already employed as mechanical actuator for coplanar wave guides up to nanometer wave range. The next step is to take advantage of the elastic behavior of this film by moving this film by electrostatic forces. The exact solution of the governing equations for laminated NRTF were stablished. The mechanical properties relations of the NRTF material were plotted and discussed. The thickness distribution across the Nano-film thickness is discussed to describe the durability under deformation with differential pressure (P). As a results, these technique is now well developed and are so mature that they become useful and rapid tools for mechanical characteristics which have been determined include a Young's modulus E_x and E_y were calculated to be 42.01 and 58.63 Gpa respectively for Nano-film material with thickness (h) 5 nm. The maximum Nano-deflection $w_{\max}$ was estimated to be 7.0527 nm was occured at the center of the NRTF. The strain in the center of NRTF was found equal 0.43504 (nm/nm) for bulging tests with applied pressure (P) 10 pa. The stress across NRTF thickness was estimated to be ±3.637 pa in tension above midplane and compression below midplane of NRTF thickness. The NRTF thickness was decreased from 5 to 4.883 nm with increased of the applied pressure (P) from 0 to 10 Pa.

References

Ahmed, M. and Hashmi, M.S.J. (1998), "Finite-element analysis of bulge forming applying pressure and in-plane compressive load", *Mater. Process. Technol.*, **77**(1), 95-102.

Alizada, A.N. and Sofiyev, A.H. (2011a), "Modified Young's moduli of nano-materials taking into account the scale effects and vacancies", *Meccanica*, **46**(5), 915-920.

Alizada, A.N. and Sofiyev, A.H. (2011b), "On the mechanics of deformation and stability of the beam with a nanocoating", *Reinf. Plastic. Compos.*, **30**(18), 1583-1595.

Alizada, A.N., Sofiyev, A.H. and Kuruoglu, N. (2012), "Stress analysis of a substrate coated by nanomaterials with vacancies subjected to uniform extension load", *Acta. Mech.*, **223**(7), 1371-1383.

Altabey, W. (2017), "A study on thermo-mechanical Behavior of MCD through bulge test analysis", *Adv. Computat. Des., Int. J.*, **2**(2), 107-119.

Brandon, J.F., Lecoanet, H. and Oytana, C. (1979), "A new formulation for the bulging of viscous sheet metals", *Int. J. Mech. Sci.*, **21**(7), 379-386.

Chater, E. and Neale, K.W. (1983), "Finite plastic deformation of a circular membrane under hydrostatic

pressure – I: Rate-independent behaviour", *Mech. Sci.*, **25**(4), 219-233.
Ebrahimi, F. and Barati, M.R. (2016b-a), "Analytical solution for nonlocal buckling characteristics of higher-order inhomogeneous nanosize beams embedded in elastic medium", *Adv. Nano Res., Int. J.*, **4**(3), 229-249.
Ebrahimi, F. and Barati, M.R. (2016a-b), "An exact solution for buckling analysis of embedded piezo-electro-magnetically actuated nanoscale beams", *Adv. Nano Res., Int. J.*, **4**(2), 65-84.
Ebrahimi, F. and Barati, M.R. (2016c), "Buckling analysis of nonlocal third-order shear deformable functionally graded piezoelectric nanobeams embedded in elastic medium", *J. Brazil. Soc. Mech. Sci. Eng.*, **39**(3), 937-952. DOI: 10.1007/s40430-016-0551-5
Ebrahimi, F. and Barati, M.R. (2016d), "Dynamic modeling of a thermo–piezo-electrically actuated nanosize beam subjected to a magnetic field", *J. Appl. Phys. A*, **122**(4), 451.
Ebrahimi, F. and Barati, M.R. (2016e), "Electromechanical buckling behavior of smart piezoelectrically actuated higher-order size-dependent graded nanoscale beams in thermal environment", *Int. J. Smart Nano Mater.*, **7**(2), 69-90.
Ebrahimi, F. and Barati, M.R. (2016f), "Small scale effects on hygro-thermo-mechanical vibration of temperature dependent nonhomogeneous nanoscale beams", *J. Mech. Adv. Mater. Struct.*, **24**(11), 924-936. DOI: http://dx.doi.org/10.1080/15376494.2016.1196795
Ebrahimi, F. and Barati, M.R. (2016g), "Vibration analysis of smart piezoelectrically actuated nanobeams subjected to magneto-electrical field in thermal environment", *J. Vib. Control*, 1077546316646239. DOI: http://dx.doi.org/10.1177/1077546316646239
Ebrahimi, F. and Barati, M.R. (2017), "Buckling analysis of smart size-dependent higher order magneto-electro-thermo-elastic functionally graded nanosize beams", *J. Mech.*, **33**(1), 23-33.
Ebrahimi, F. and Farzamand, N. (2016), "Thermo-mechanical vibration analysis of sandwich beams with functionally graded carbon nanotube-reinforced composite face sheets based on a higher-order shear deformation beam theory", *J. Mech. Adv. Mater. Struct.*, **24**(10), 820-829. DOI: http://dx.doi.org/10.1080/15376494.2016.1196786
Ebrahimi, F. and Salari, E. (2015a), "Effect of various thermal loadings on buckling and vibrational characteristics of nonlocal temperature-dependent FG nanobeams", *J. Mech. Adv. Mater. Struct.*, **23**(12), 1-58.
Ebrahimi, F. and Salari, E. (2015b), "Size-dependent thermo-electrical buckling analysis of functionally graded piezoelectric nanobeams", *J. Smart Mater. Struct.*, **24**(12), 125007.
Ebrahimi, F. and Shafiei, N. (2016), "Influence of initial shear stress on the vibration behavior of single-layered graphene sheets embedded in an elastic medium based on Reddy's higher-order shear deformation plate theory", *J. Mech. Adv. Mater. Struct.*, **24**(9), 761-772. DOI: http://dx.doi.org/10.1080/15376494.2016.1196781
Ebrahimi, F., Salari, E. and Hosseini, S.A.H. (2015), "Thermomechanical vibration behavior of FG nanobeams subjected to linear and non-linear temperature distributions", *J. Thermal Stresses*, **38**(12), 1360-1386.
Edwards, R.L., Coles, G. and Sharpe, W.N. (2004), "Comparison of tensile and bulge tests for thin-film silicon nitride", *Soc. Experim. Mech.*, **44**(1), 49-54.
Gologranc, F. (1975), "Beitrag zur Ermittlung von Fließkurven im kontinuierlichen hydraulischen Tiefungsversuch (Evaluation of the flow stress curve with the continuous hydraulic bulge test)", Dissertation; Institute for Metal Forming Technology, University of Stuttgart, Germany.
Grolleau, V., Gary, G. and Mohr, D. (2008), "Biaxial testing of sheet materials at high strain rates using viscoelastic bars", *Experim. Mech.*, **48**(3), 293-306.
Hill, R. (1950), "A theory of plastic bulging of a metal diaphragm by lateral pressure", *The London, Edinburgh, and Dublin Philosophical Magazine and Journal of Science*, **41**(322), 1133-1142.
Hill, R. (1990), "Constitutive modelling of orthotropic plasticity in sheet metals", *Mech. Phys. Solids.*, **38**(3), 405-417.
Huang, A.W., Lu, C.H., Wu, S.C., Chen, T.C., Vinci, R.P., Brown, W.L. and Lin, M.T. (2016), "Viscoelastic mechanical properties measurement of thin Al and Al-Mg films using bulge testing ", *Thin*

Solid Films, **618**, 2-7. DOI: 10.1016/j.tsf.2016.03.064
Ilahi, M.F. and Paul, T.K. (1985), "Hydrostatic bulging of a circular soft brass diaphragm", *Int. J. Mech. Sci.* **27**(5), 275-280.
Ilahi, M.F., Parmar, A. and Mellor, P.B. (1981), "Hydrostatic bulging of a circular aluminum diaphragm", *Mech. Sci.*, **23**(4), 221-227.
Itozaki, H. (1982), "Mechanical properties of composition modulated copper-palladium foils", Ph.D. Dissertation; Northwestern University, Evanston, IL, USA.
Jung, B., Lee, H., Hwang, K. and Park, H. (2012), "Measurement of mechanical properties of thin films using a combination of the bulge test and nanoindentation", *Transact. Kor. Soc. Mech. Engr. B*, **36**(2), 117-123.
Jung, B., Lee, H., Hwang, K. and Park, H. (2013), "Observation of size effect and measurement of mechanical properties of Ti thin film by bulge test", *Transact. Kor. Soc. Mech. Engr. B*, **37**(1), 19-25.
Kular, G.S. and The, J.H.L. (1972), "The bulging of anisotropic aluminum sheets – A comparison of theory and experiments", *Int. J. Mach. Tool Des. Res.*, **12**(4), 281-296.
Mellor, P.B. (1956), "Stretch forming under fluid pressure", *Mech. Phys. Solid.*, **5**(1), 41-56.
Panknin, W. (1959), "Der hydraulische Tiefungsversuch und die Ermittlung von Fließkurven (The hydraulic bulge test and the determination of the flow stress curves)", Dissertation; Institute for Metal Forming Technology, University of Stuttgart, Germany.
Small, M.K. and Nix, W.D. (1992), "Analysis of the accuracy of the bulge test in determining the mechanical properties of thin-films", *Mater. Res.*, **7**(6), 1553-1563.
Storakers, B. (1966), "Finite plastic deformation of a circular membrane under hydrostatic pressure", *Mech. Sci.*, **8**(10), 619-628.
Suttner, S. and Merklein, M. (2016), "Experimental and numerical investigation of a strain rate controlled hydraulic bulge test of sheet metal", *Mater. Process. Technol.*, **235**, 121-133.
Tabata, O., Kawahata, K., Sugiyama, S. and Igarashi, I. (1989), "Mechanical property measurements of thin films using load-deflection of composite rectangular membranes", *J. Sensors Actuat.*, **20**(1-2), 135-141.
Tang, S.C. (1982), "Large strain analysis of an inflating membrane", *Comput. Struct.*, **15**(1), 71-78.
Wan, K., Guo, S. and Dillard, D.A. (2003), "A theoretical and numerical study of a thin clamped circular film under an external load in the presence of a tensile residual stress", *Thin Solid Films*, **425**(1), 150-162.
Vlassak, J.J. (1994), "New experimental techniques and analysis methods for the study of mechanical properties of materials in small volumes", Ph.D. Dissertation; Stanford University, Stanford, CA, USA.
Vlassak, J.J. and Nix, W.D. (1992), "A new bulge test technique for the determination of Young's modulus and Poisson's ratio of thin films", *J. Mater. Res.*, **7**(12), 3242-3249.
Wang, N.M. and Shammamy, M.R. (1969), "On the plastic bulging of a circular diaphragm by hydrostatic pressure", *Mech. Phys. Solids*, **17**(1), 43-64.
Xiang, Y., Chen, X. and Vlassak, J.J. (2005), "Plane-strain bulge test for thin films", *Mater. Res. Soc.*, **20**(9), 2360-2370.
Yang, L., Long, S., Ma, Z. and Wang, Z. (2014), "Accuracy analysis of plane-strain bulge test for determining mechanical properties of thin films", *Transact. Nonferrous Metals Soc. China*, **24**(10), 3265-3273.
Zeghloul, A., Mesrar, R. and Ferron, G. (1991), "Influence of material parameters on the hydrostatic bulging of a circular diaphragm", *Mech. Sci.*, **33**(3), 229-243.
Zhang, J., Sun, Y., Li, D., Cao, Y., Wang, Z., Ma, J. and Zhao, G. (2015), "Modeling the mechanics of graphene-based polymer composite film measured by the bulge test", *Phys. D: Appl. Phys.*, **48**(42), 425302.

JL